Please cite this article in press as: Myers et al., Mesoscale Modeling of Nucleosome-Binding Antibody PL2-6: Mono- versus Bivalent Chromatin Complexes, Biophysical Journal (2020), https://doi.org/10.1016/j.bpj.2019.08.019

Biophysical *Journal*
Article

Biophysical Society

Mesoscale Modeling of Nucleosome-Binding Antibody PL2-6: Mono- versus Bivalent Chromatin Complexes

Christopher G. Myers,[1] Donald E. Olins,[2] Ada L. Olins,[2] and Tamar Schlick[1,3,4,*]
[1]Department of Chemistry, New York University, New York, New York; [2]Department of Pharmaceutical Sciences, College of Pharmacy, University of New England, Portland, Maine; [3]Courant Institute of Mathematical Sciences, New York University, New York, New York; and [4]New York University-East China Normal University Center for Computational Chemistry at New York University Shanghai, Shanghai, China

ABSTRACT Interactions of chromatin with bivalent immunoglobin nucleosome-binding antibodies and their monovalent (papain-derived) antigen-binding fragment analogs are useful probes for examining chromatin conformational states. To help interpret antibody-chromatin interactions and explore how antibodies might compete for interactions with chromatin components, we incorporate coarse-grained PL2-6 antibody modeling into our mesoscale chromatin model. We analyze interactions and fiber structures for the antibody-chromatin complexes in open and condensed chromatin, with and without H1 linker histone (LH). Despite minimal and transient interactions at physiological salt, we capture significant differences in antibody-chromatin complex configurations in open fibers, with more intense interactions between the bivalent antibody and chromatin compared to monovalent antigen-binding fragments. For these open chromatin fiber morphologies, antibody binding to histone tails is increased and compaction is greater for bivalent compared to monovalent and antibody-free systems. Differences between monovalent and bivalent binding result from antibody competition with internal chromatin fiber components (nucleosome core and linker DNA) for histone tail (H3, H4, H2A, H2B) interactions. This antibody competition for tail contacts reduces tail-core and tail-linker interactions and increases tail-antibody interactions. Such internal structural changes in open fibers resemble mechanisms of LH condensation, driven by charge screening and entropy changes. For condensed fibers at physiological salt, the three systems are much more similar overall, but some subtle tail interaction differences can be noted. Adding LH results in less-dramatic changes for all systems, except that the bivalent complex at physiological salt shows cooperative effects between LH and the antibodies in condensing chromatin fibers. Such dynamic interactions that depend on the internal structure and complex-stabilizing interactions within the chromatin fiber have implications for gene regulation and other chromatin complexes such as with LH, remodeling proteins, and small molecular chaperones that bind and modulate chromatin structure.

SIGNIFICANCE Using mesoscale modeling, we help interpret different binding modes for antibody-chromatin interactions between monovalent and bivalent forms of the PL2-6 antibody. To our knowledge, this is the first application of a coarse-grained computational antibody model to probe chromatin structure and mechanisms of antibody-chromatin binding. Our work emphasizes how antibody units compete with native internal chromatin fiber units (histone tails, nucleosome core, and linker DNA) for fiber-stabilizing interactions and thereby drive differential antibody binding for open zigzag chromatin fibers. Such competition, which dynamically alters internal chromatin structure upon binding, is relevant to other chromatin-binding mechanisms such as those involving linker histones, small molecular chaperones, and chromatin-remodeling proteins.

INTRODUCTION

Antibodies that bind DNA and/or nucleosomes (termed anti-DNA and anti-nucleosome) have been used for many basic research and medical applications (1). For example, anti-nucleosome antibodies like monoclonal antibody (mAb) PL2-6, belonging to the immunoglobin (IgG) class of antibodies, serve as general probes for chromatin states (2). It is well-known that chromatin states can be modulated by linker histone (LH) (3), protein remodelers (4), and other molecules that alter chromatin structure both locally and globally (5). Understanding these chromatin states and the

Submitted April 12, 2019, and accepted for publication August 15, 2019.
*Correspondence: schlick@nyu.edu
Editor: Toshio Tsukiyama.
https://doi.org/10.1016/j.bpj.2019.08.019

Please cite this article in press as: Myers et al., Mesoscale Modeling of Nucleosome-Binding Antibody PL2-6: Mono- versus Bivalent Chromatin Complexes, Biophysical Journal (2020), https://doi.org/10.1016/j.bpj.2019.08.019

transitions among states along developmental, transcriptional, and other biological pathways has been a formidable challenge addressed by many experimental and computational approaches on the level of nucleosomes, fibers, genes, and chromosomes (6). Our group has contributed to these efforts by nucleosome-resolution views of fibers and genes in collaboration with experimentalists (7).

Here, we study, using coarse-grained techniques, antibody-chromatin interactions to interrogate how antibody systems interact with fiber systems. Such antibody-chromatin interactions have applications in diagnostics and therapeutic approaches (8,9) and are thus important to characterize. Antibody-chromatin systems have also been used in recent experiments using the bivalent form of the PL2-6 antibody to detect an "exposed" chromatin epitope (2,10). This exposed epitope-rich region (denoted "epichromatin") is concentrated on the surface of chromatin beneath the interphase nuclear envelope and at the "outer" surface of clustered mitotic chromosomes within fixed and permeabilized cells. In contrast, the monovalent "Fab" form of PL2-6 stains chromatin throughout cell nuclei. These staining patterns suggest different binding modes between the monovalent and bivalent PL2-6 forms (Fig. 1 *A*). The "epichromatin hypothesis" proposes that epichromatin reflects a unique, evolutionarily conserved conformation of fixed chromatin that facilitates interaction with the nuclear envelope and a geometrically driven specific binding of bivalent PL2-6 (2).

An x-ray crystal structure for PL2-6 is not available, but a sequence-based homology model for the Fab subunit was derived (Robyn Stanfield, personal communication). We use this model here (Fig. 1 *B*) to develop coarse-grained models of both the monovalent and bivalent forms of PL2-6. We denote the full IgG structure (Fig. 1 *C*) as "bivalent." The "monovalent" Fab form is derived via papain digestion through cleavage of the Fab arms from the Fc region of the full bivalent IgG structure. Both the bivalent PL2-6 (11) and (papain-derived) monovalent Fab (12) have been shown to bind mononucleosomes in solution. Interpreting the staining patterns associated with the epichromatin hypothesis would require modeling rigid chromatin in the crowded cellular milieu to flexible antibodies. As a first step, however, for exploring the general interaction of antibody systems with chromatin fibers, we analyze coarse-grained complex structures and energetics by comparing systems of bivalent versus monovalent PL2-6 antibodies bound to flexible chromatin fibers.

Specifically, we combine coarse-grained modeling of PL2-6 antibodies with our mesoscale chromatin model to elucidate differences in the structures and binding of chromatin fibers, comparing bivalent versus monovalent PL2-6 chromatin complexes to one another and to antibody-free

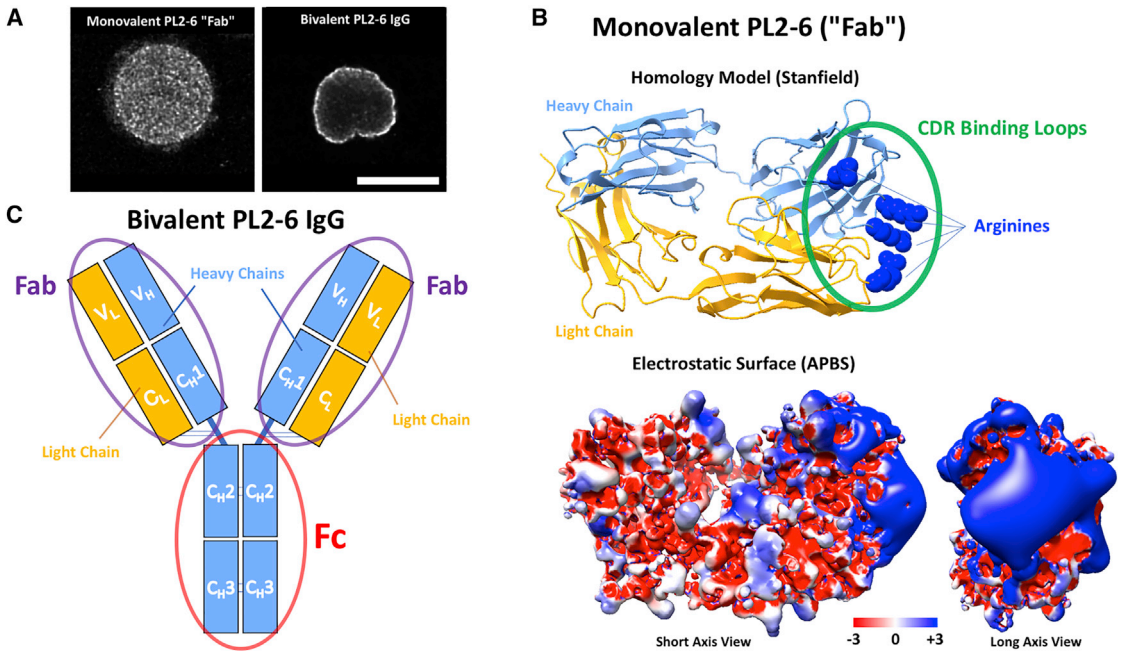

FIGURE 1 Monovalent and bivalent forms of PL2-6 antibody. (*A*) Differential staining patterns observed between two forms of PL2-6 suggest differential binding modes to chromatin for each form. Monovalent PL2-6 Fab stains across entire cell nuclei, whereas the bivalent PL2-6 produces a ring-like staining pattern localized near the nuclear envelope (2). Scale bar, 10 μm. (*B*) The PL2-6 Fab subunit homology model provided by Robyn Stanfield is shown, composed of heavy (*blue*) and light (*orange*) chains and used to calculate the Fab electrostatic surface using Adaptive Poisson-Boltzmann Solver software (22,23) at pH 7.0. The binding region contains a positive charge distribution due largely to arginine residues (*blue*) within the CDR binding loops (*circled* in *green*). (*C*) A schematic representation of the bivalent IgG structure of PL2-6 is shown, composed of two Fab subunits (*circled* in *purple*) and an Fc region (*circled* in *red*) composed of conserved (C_H1, C_H2, C_H3, C_L) and variable (V_H, V_L) regions within light (*orange*) and heavy (*blue*) chains; adapted from *Antibody Molecular Structure* (16). To see this figure in color, go online.

Please cite this article in press as: Myers et al., Mesoscale Modeling of Nucleosome-Binding Antibody PL2-6: Mono- versus Bivalent Chromatin Complexes, Biophysical Journal (2020), https://doi.org/10.1016/j.bpj.2019.08.019

systems. We show that competition with internal chromatin elements for histone tail interactions leads to different conformations of these three systems. Low-salt chromatin complexes with bivalent PL2-6 are more compact and show stronger interactions with the histone tails through mechanisms of charge screening and increased entropic contributions compared to monovalent PL2-6 complexes. Both antibody systems, especially the bivalent system, capture antibody interactions with all histone tails. In particular, antibodies compete with linker DNA for H3 and $H2A_1$ (or N-terminal H2A) interactions and with cores for all tail interactions, notably H4, H2B, and $H2A_2$ (or C-terminal H2A). Such mechanisms resemble H1 LH-induced chromatin condensation, with similar changes in tail contacts and internal fiber structure. For condensed chromatin fibers at physiological salt, monovalent and bivalent PL2-6 interact transiently and modify long-range internucleosomal interactions modestly. Monovalent PL2-6 has only minimal changes in $H2A_1$ tails compared to antibody-free systems, whereas bivalent PL2-6 decreases H3 and H4 interactions with nonparental cores.

The overall results are only modestly affected by introducing LH into our complexes because LH compaction dominates over antibody compaction. At low-salt conditions, LH tends to decrease overall interactions with monovalent and bivalent PL2-6 through charge screening and steric interference, thus minimizing differences between monovalent and bivalent complexes. At physiological salt, monovalent PL2-6 and LH act in opposition, with the overall effect of decreasing compaction and H3 and H4 tail interactions with nonparental cores. On the other hand, bivalent PL2-6 and LH act cooperatively to increase H3 and H4 interactions with nonparental cores to produce more condensed fibers.

Overall, the competition we discuss is relevant to other chromatin complexes such as LH (13,14) and to using antibodies as probes for chromatin conformations and therapeutic agents. Further modeling development and new experiments could also help interpret and test the epichromatin hypothesis.

MATERIALS AND METHODS

Antibody system

PL2-6 belongs to the IgG subclass of immunoglobin antibodies (15). The full IgG structure (Fig. 1 *C*) consists of two antigen-binding fragment (Fab) arms joined together by a crystallizable fragment (Fc) connector region. Each Fab arm contains identical complementarity determining regions (CDRs) that facilitate the highly specific binding to the antibody's preferred epitope target (16). Sequence homology within PL2-6's CDR loops with centromere protein C1 (CENP-C) (17) and latency-associated nuclear antigen (LANA) (18–20) suggests that PL2-6 binds the nucleosome at the "acidic patch." The acidic patch is a negatively charged region found on both sides of the symmetric nucleosomal core particle that is defined by six amino acid residues of the H2A/H2B histones (17,20). The acidic patch regulates chromatin higher-order structure via the histone H4 N-terminal tail domain interactions with neighboring nucleosome core particles (NCPs) at the acidic patch. The acidic-patch region is considered crucial for chromatin remodeling, with important implications for gene regulation and cancer biology (21).

Using the homology model provided by Robyn Stanfield, we perform electrostatic calculations using the Adaptive Poisson-Boltzmann Solver software (22,23) to determine an electrostatic surface for the PL2-6 Fab (Fig. 1 *B*). Arginines within the CDR loops (conserved in both CENP-C and LANA) create a positive charge distribution at the binding end of the Fab subunit (*green circles*). This suggests that the energetics of Fab binding and stabilization with chromatin depend heavily on electrostatic interactions between this positive charge distribution and the negatively charged linker DNA and acidic patches of chromatin. A coarse-grained electrostatic model of the antibody protein should thus capture significant aspects of chromatin interactions leading to binding. The CDR binding loops of monovalent and bivalent PL2-6 (Fig. 1 *C*, *circled* in *green*) share the -LDYW- motif that facilitates CENP-C interaction with the acidic patch upon nucleosomal binding, which may stabilize the final chromatin complex conformations of PL2-6. However, internal interactions of the chromatin fiber could preemptively change the energetic landscape before antibody binding. Moreover, monovalent and bivalent antibodies may follow different mechanistic pathways toward a final binding to the acidic patch.

Mesoscale chromatin model

We simulate chromatin fibers with our mesoscale chromatin model (Fig. 2 *A*) (24–26) consisting of four components: coarse-grained beads of linker DNA, electrostatically charged NCPs, coarse-grained beads for flexible histone tails, and beads for H1 LH. Each NCP consist of 300 partial point charges that approximate the core electrostatic surface determined by applying our discrete surface charge optimization algorithm (27,28) to the NCP crystal structure (29). NCPs are joined by linker DNA modeled as a modified worm-like chain of beads that each represent about nine basepairs (bp). LH (based on rat H1.4 (30,31)) is modeled as a rigid body of 28 beads using the united atom model (13), with 22 beads for the C-terminal domain (CTD) and six beads for the globular head inserted on the dyad axis. For more details of our LH model, see Luque et al. (13). In this study, we simulate fiber systems of 24 nucleosomes and include simulations with LH in the Supporting Materials and Methods. Equilibrium MC simulations with LH contain 24 linker histones at a total density ρ of one LH per NCP. All nonbonded interactions in the system are modeled with excluded-volume terms via 12-6 Lennard-Jones van der Waals (VdW) potential and screened electrostatic Debye-Hückel energy terms

$$\mathrm{E_{Fab}} = \sum_{i=1}\sum_{j>i}\left[\underbrace{k_{ij}\left[\left(\frac{\sigma_{ij}}{r_{ij}}\right)^{12} - \left(\frac{\sigma_{ij}}{r_{ij}}\right)^{6}\right]}_{VdW} + \underbrace{\frac{kq_iq_j}{4\pi\epsilon\epsilon_0 r_{ij}}e^{-\kappa r_{ij}}}_{Elec}\right], \quad (1)$$

where σ_{ij} is the effective Lennard-Jones VdW diameter of the two interacting beads in nanometers and k_{ij} is an energy parameter that controls the steepness of the excluded-volume potential, $\epsilon_r = 88.9$ is the relative dielectric of water, and ϵ_0 is the permittivity of free space and using a Debye screening length $\kappa = 0.736\sqrt{(C_S/0.05)(298/T)}nm^{-1}$ at $T = 298$ K and monovalent salt concentration C_S. There are five types of Monte Carlo (MC) moves in the chromatin system: a global pivot move, a configurationally biased tail Rosenbluth regrow move, local rotation and translation moves for nucleosomes and linker DNA, and for simulations including LH, translation of the LH CTD. All moves are accepted or rejected according to the Metropolis algorithm acceptance criterion with Boltzmann-weighted probabilities from the total system energy and temperature. For full details of the model, see Bascom et al. (32).

Please cite this article in press as: Myers et al., Mesoscale Modeling of Nucleosome-Binding Antibody PL2-6: Mono- versus Bivalent Chromatin Complexes, Biophysical Journal (2020), https://doi.org/10.1016/j.bpj.2019.08.019

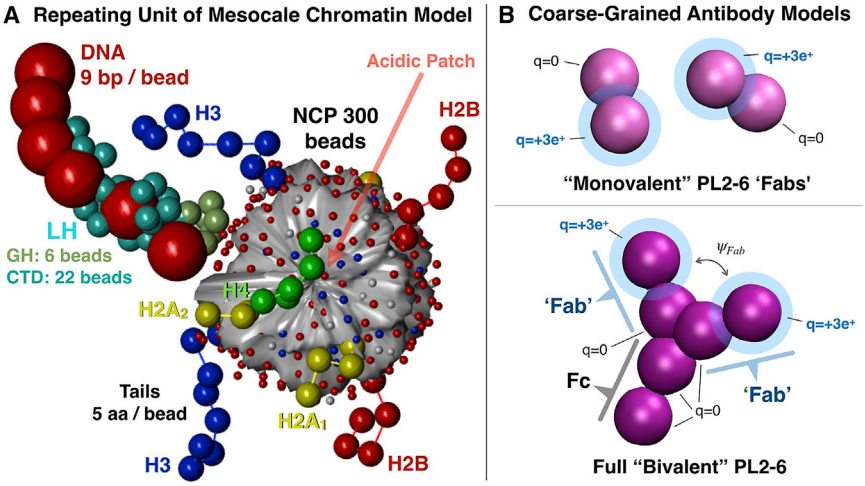

FIGURE 2 Mesoscale chromatin and coarse-grained antibody models. (*A*) Our chromatin mesoscale model repeating unit consists of a single nucleosome core particle (NCP) with 300 charged beads and flexible histone tails (five amino acids per bead), joined to nearest neighbor NCPs by linker DNA (nine bp per bead). Linker histone (LH) consists of a CTD and a globular head. $H2A_1$ and $H2A_2$ denote H2A N- and C termini, respectively. See details in Bascom et al. (32). (*B*) Our coarse-grained rigid-body model for monovalent PL2-6 Fab contains two beads. The bivalent PL2-6 model has two Fab arms connected by a two-bead Fc connector (with same dimensions as Fabs) for a total of six beads. Positively charged spheres (highlighted in *blue*) are assigned Debye-Hückel-screened surface charges $q_{Fab} = +3e$ at the binding ends in both models. To see this figure in color, go online.

Coarse-grained antibody model

We have devised and employed coarse-grained models (Fig. 2 *B*) for both monovalent and bivalent PL2-6 antibody structures to simulate in conjunction with our mesoscale chromatin model. Such a coarse-grained bivalent antibody model is similar to previous models for IgG antibodies (33–35). To our knowledge, this is the first application of such a model to investigate antibody binding to chromatin or chromatin structure.

In both our coarse-grained antibody models (Fig. 2 *B*), the Fab and Fc regions are modeled separately as two rigidly connected spherical beads with volume exclusion and surface charges that interact with the beads of the chromatin fiber and the other antibodies according to the energy terms

$$E_{Fab} = \sum_{i=1}\sum_{j>i}\left[\underbrace{0.5(\epsilon_i+\epsilon_j)\left[\left(\frac{0.5(\sigma_i+\sigma_j)}{r_{ij}}\right)^{12}-\left(\frac{0.5(\sigma_i+\sigma_j)}{r_{ij}}\right)^{6}\right]}_{VdW}+\underbrace{\frac{kq_iq_j}{4\pi\epsilon\epsilon_0 r_{ij}}e^{-\kappa r_{ij}}}_{Elec}\right], \quad (2)$$

where $\epsilon_i = k_bT$ and $\sigma_i = 4.0$ nm is the Lennard-Jones VdW diameter for beads approximating the dimensions of the Fab and Fc regions; q_i is the charge of each antibody bead interacting with each other bead in the chromatin-antibody system according to their values of ϵ_j, σ_j, q_j; and with electrostatic constants as defined in Eq. 1. The monovalent antibody consists of two rigidly connected beads. The bivalent consists of a total of six beads of the rigidly connected Fab, Fab, and Fc regions. Each bead is assigned a surface charge q_i (monovalent: $i = 1,2$; bivalent: $i = 1,2,\ldots,6$), which interacts with all other pairwise nonbonded charged beads of q_j and σ_j via Eq. 2 and according to our previously developed chromatin model. We employ a charge of $q_{Fab} = +3e$ to approximate the charge of the Fab binding region containing the specific CDR loops and the three arginines mentioned above and thus assign $q_i = q_{Fab} = +3e$ to a single bead in the monovalent Fab and to the end of the two-bead Fab groups in the bivalent PL2-6 (Fig. 2 *B*, charged beads highlighted in *blue*). Thus, the entire bivalent antibody has a combined net charge of $q = +6e$.

Bivalent IgG hinges connecting Fc and Fab regions are generally flexible, and studies have shown that rigid models can significantly decrease binding compared to flexible models (36). Other studies, however, have shown that experimental properties like osmotic compressibility, as measured by high-concentration Rayleigh scattering, were not altered by hinge flexibility (34); subsequent studies have ignored flexibility in favor of a rigid model for improved computational convergence and simplicity (33). Furthermore, the IgG2 subclass that contains PL2-6 has both the shortest hinges among all IgGs as well as additional rigidity because of a polyproline helix stabilized by up to four additional inter-heavy-chain disulfide bridges (37). Therefore, we model both the monovalent and bivalent antibodies as rigid molecules as a reasonable first approximation.

For the rigid bivalent IgG, we fix the "Fab angle" ψ_{Fab} at an equilibrium angle of $\psi_0 = 68°$, used in previous IgG models and based on representative values from mAB crystal structures (34). Our bivalent model is constrained to be planar and rigid in the Fab and Fc connector regions which rotate freely in 3D space with orientations defined by three internal Euler angles α_i, β_i, γ_i ($i = 1,2,..,N$ for N antibodies).

The antibodies move within the chromatin system according to two additional MC antibody translation and rotation moves, accepted or rejected according to the same Metropolis algorithm acceptance criterion with the Boltzmann-weighted probability from the total system energy and temperature. Thus, in bivalent and monovalent antibody/chromatin systems with LH, we employ a total of seven MC moves: the five chromatin moves mentioned above and these two additional antibody moves. In the absence of LH, there is one less relevant move.

In the Supporting Materials and Methods, we include preliminary results of a flexible bivalent PL2-6 IgG model that allows the Fab angle ψ_{Fab} to vary randomly around the equilibrium Fab angle ψ_0 of the rigid model. We show representative structures comparing rigid and bivalent chromatin systems at low and physiological salt in Fig. S5. We compare results of our rigid to flexible models for chromatin interactions in Figs. S8 and S10. For these flexible bivalent PL2-6 systems, we incorporate one additional MC move that allows the Fab angle ψ_{Fab} to randomly vary within the PL2-6

Please cite this article in press as: Myers et al., Mesoscale Modeling of Nucleosome-Binding Antibody PL2-6: Mono- versus Bivalent Chromatin Complexes, Biophysical Journal (2020), https://doi.org/10.1016/j.bpj.2019.08.019

plane up to $\pm 30^{\circ}$ around the equilibrium angle $\psi_0 = 68^{\circ}$. We find that the behavior of chromatin systems with flexible bivalent PL2-6 is qualitatively similar to the rigid model. The flexible model binds chromatin slightly less tightly (Fig. S5), with a modest decrease in overall interactions with tails, cores, and linker DNA (Figs. S8 and S10). These preliminary results indicate that our rigid model is reasonable as a first-order approximation. Indeed, differences between the monovalent and bivalent antibodies and respective complexes appear more important than the internal treatment of the antibody themselves.

Simulation parameters

Idealized zigzag starting structures of 24 nucleosomes and a nucleosome repeat length (equal to 147 bp plus length of linker DNA) of 200 bp were used for all chromatin fibers, corresponding to a common nucleosome repeat length for human cells (Fig. S1). For simulations containing antibodies, we introduce monovalent and bivalent antibodies at starting configurations distributed at a distance of 100 nm evenly along the fiber structure for a total of 72 antibodies (Figs. S2 and S3). To prevent diffusion of the antibody molecules away from the fiber without imposing any artificial forces on the system, we employ periodic boundary conditions inside a 400-nm box centered around the chromatin fiber. All simulations were conducted for a minimum of 20 million MC steps.

Data analysis

Interactions (f_{inter}) between all chromatin elements and antibodies are evaluated by measuring the number of simulation frames for which pairwise distances between elements are within 5 nm, sampled over the last 1 million frames of the simulation and normalized across all sampled frames. Tail interactions are averaged over both copies of each N-terminal tail for H3, H4, and H2B. $H2A_1$ and $H2A_2$ denote N-terminal and C-terminal H2A tails, respectively. Distances are measured from the center of the end tail bead, from the geometric center of the entire nucleosome core, from the center of each linker bead, and from the center of the charged beads in both monovalent and bivalent systems.

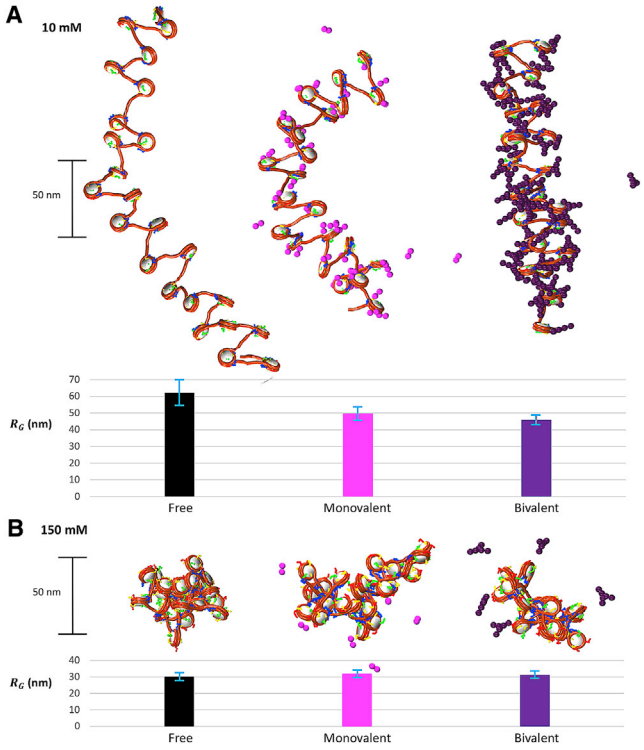

FIGURE 3 Snapshots of representative fibers from six antibody/chromatin systems. All fibers consist of 24 nucleosomes and start from idealized zigzag configurations (Figs. S1 and S2). For each condition (low salt or physiological salt), we show results for free fiber, monovalent PL2-6 Fab complex, and bivalent PL2-6 complex without LH. Radii of gyration (R_G) of chromatin fibers are shown in nanometers for free (*black*), monovalent (*magenta*), and bivalent (*purple*) systems. (*A*) Low salt and (*B*) physiological salt are shown, both without LH. To see this figure in color, go online.

RESULTS

Overall behavior

We simulate three categories of chromatin systems: free chromatin reference systems, monovalent PL2-6 with chromatin, and bivalent PL2-6 with chromatin. For each of these categories, we simulate at both low and physiological monovalent salt concentrations ($C_S = 10$ and $C_S = 150$ mM, respectively). Representative structures from each of these six systems without LH are shown in Fig. 3 with radii of gyration averaged over the last 5 million steps and SD as blue error bars. We show the same for these six systems simulated with LH in Fig. S4 because the relative trends are similar. For open fiber morphologies under low-salt conditions, we observe much more intense binding in bivalent versus monovalent complexes (Fig. 3 *A*). This striking difference between the middle (monovalent) and right (bivalent) complexes in Fig. 3 *A* is counterintintuitive. For condensed fibers at physiological salt, we find that antibody binding to chromatin fibers is highly dynamic and transient (Fig. 3 *B*). A similar difference for all three systems occurs in the presence of LH (Fig. S4), although overall compaction is greater, as expected (smaller R_G).

In more detail, at low salt (Fig. 3 *A*), both monovalent and bivalent antibodies help condense chromatin fibers, with significantly reduced radii of gyration for monovalent systems compared to antibody-free and bivalent compared to monovalent systems. Furthermore, fibers with PL2-6 are stiffer, with less variability in the radii of gyration, reflected in lower SDs (*blue bars*) compared to free chromatin. This behavior resembles synergistic mechanisms of dynamic condensation regulated by LH (13) through internal mechanisms discussed below (Tail Interactions). As with LH-induced condensation, the positively charged PL2-6 antibodies neutralize the negative charge of linker DNA and alter internal native chromatin contacts. With bivalent PL2-6's greater positive charge and tighter binding, we observe further compaction in bivalent compared to monovalent complexes (Fig. 3 *A*). In the presence of LH, all systems of fibers are more compact compared to low salt, consistent with previous studies (13), with smaller sensitivity to antibody presence or type (Fig. S4).

Similarly, at physiological salt (Fig. 3 *B*), all systems of fibers are more compact compared to low salt, as found previously (24,38), and thus also less sensitive to antibody type. Without LH, however, both monovalent and bivalent PL2-6 complexes are less condensed compared to antibody-free systems (Fig. 3 *B*) because of internal mechanisms discussed below. With LH, however, we observe opposing mechanisms: monovalent PL2-6 decreases compaction, whereas bivalent PL2-6 works cooperatively with LH and results in the most compact fibers (Fig. S4). Such configurational changes are brought about through a shift in internucleosomal chromatin contacts discussed below.

In the next section, we focus on "open" chromatin fibers at low salt because they are more statistically reliable in yielding analyses of internal chromatin interactions with monovalent versus bivalent antibodies. We compare the changes in internal chromatin contacts between free, monovalent, and bivalent systems to elucidate the changes in internal chromatin structure that account for these observed binding differences.

Open zigzag fibers

Acidic-patch affinity greater in monovalent versus bivalent PL2-6 because of increased core affinity

We analyze open fibers at low salt to determine whether antibody type and chromatin binding affect the relative acidic-patch affinities of PL2-6. Because PL2-6 is expected to bind to the acidic patch (12), it is plausible that conformational differences in bivalent and monovalent chromatin complexes reflect variations in acidic-patch availabilities, which might account for the tighter chromatin binding observed for the bivalent complex. To compare acidic-patch affinities between bivalent and monovalent PL2-6 relative to other regions of the nucleosome core, we measure interactions between the antibodies' binding regions (charged spheres) with three selected beads (Fig. 4, *black circles*), each representing a separate region on the nucleosome surface: the two acidic patches (on the front and back of the nucleosome surface, denoted Acidic Patches 1 and 2, colored *red* and *dark red*, respectively) and (as a control) the largest concentration of positive charge on the nucleosome as defined by the charges in our discretized model (denoted "Core Max (+)" and colored *blue*). The positions of the acidic patches are defined in our model by the center of the most negatively charged bead on either side of the nucleosome disk. Interactions are measured by counting pairwise distances within a 5-nm cutoff over the final million MC steps of the simulation. From Fig. 4, we see similar contacts with the three regions for all three systems, perhaps because of the coarse-grained aspect of the model. We also note a lower acidic-patch affinity for bivalent PL2-6 compared to monovalent Fab. This likely results from other stabilizing interactions in the bivalent complex (see below). We find similar results in the presence of LH (Fig. S6). Thus, although localized acidic-patch availability relative to other core regions does not account for observed differential binding of monovalent versus bivalent PL2-6, acidic-patch interactions are present in both.

Next, in Fig. 5, we examine overall changes in the internal chromatin structure between bivalent versus monovalent PL2-6 complexes in open chromatin fibers. As suggested by the decreased affinity across core regions for bivalent versus monovalent PL2-6 in Fig. 4, overall interactions of PL2-6 with nucleosome cores (*blue histograms*) are decreased compared to monovalent PL2-6. These differences suggest that significant conformational differences between the monovalent and bivalent PL2-6 explain behavior patterns. Overall, the increased histone tail interactions (*gray*) of bivalent versus monovalent explains the tighter chromatin binding of bivalent PL2-6 at low salt.

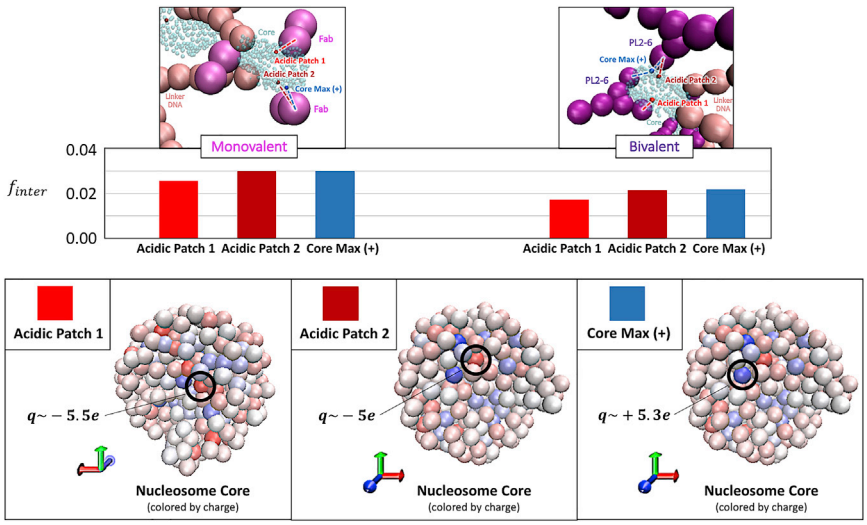

FIGURE 4 PL2-6 interactions with specific regions of the nucleosome core. The three regions are the two sides of the negatively charged acidic patch (arbitrarily labeled as Acidic Patch 1 and 2) and the largest positive charge on the nucleosome surface (Core Max (+)). Interaction frequencies (f_{inter}) are evaluated by measuring the number of simulation frames for which pairwise distances between elements are $\leq$5 nm, sampled over the last 1 million frames of the simulation and normalized across all sampled frames. Pairwise distances are measured from the center of the specified charged bead on the nucleosome core and from the center of the charged beads in both monovalent and bivalent systems. Acidic Patch 1 (*red*), Acidic Patch 2 (*dark red*), Core Max (+) Charge (*blue*). To see this figure in color, go online.

Please cite this article in press as: Myers et al., Mesoscale Modeling of Nucleosome-Binding Antibody PL2-6: Mono- versus Bivalent Chromatin Complexes, Biophysical Journal (2020), https://doi.org/10.1016/j.bpj.2019.08.019

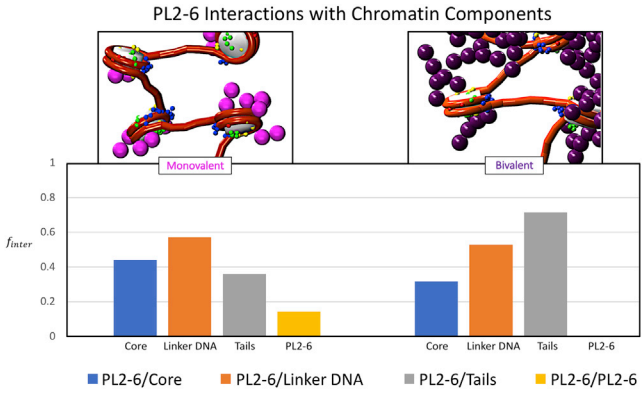

FIGURE 5 Overall antibody interactions with elements of open chromatin fiber (cores, DNA linkers, tails, and other PL2-6 antibodies) at low salt without LH. Interactions (f_{inter}) are evaluated by measuring the number of simulation frames for which pairwise distances between elements are $\leq$5 nm, sampled over the last 1 million frames of the simulation and normalized across all sampled frames. Interactions are averaged over all elements in the fiber for each category (core, linkers, tails, Fabs). Pairwise distances are measured from the center of the end tail bead, from the geometric center of the entire nucleosome core, from the center of each linker bead, and from the center of the charged beads in both monovalent and bivalent systems. To see this figure in color, go online.

This large increase in unfavorable electrostatic interactions between positively charged histone tails and positively charged PL2-6 units suggests that entropic differences between bivalent and monovalent complexes may drive these differences in binding. As large energetic differences are not observed between monovalent and bivalent complexes, the greater rotational degrees of freedom of the bivalent PL2-6 may lower the free energy of the system through increased entropy of histone tail binding compared to monovalent PL2-6.

We see similar behavior in the presence of LH (Fig. S7), but with the overall level of interactions reduced in both monovalent and bivalent systems. Thus, with LH, the competition for tail interactions between PL2-6 and Fab is reduced, lowering the accessibility to PL2-6 binding, particularly for the bivalent system. In the next section, we look more specifically at the changes in the internal chromatin tail interactions that drive differential binding and conformational changes. Preliminary results with the flexible bivalent PL2-6 show similar conformational trends for the three systems (Fig. S5).

Tail interactions

Finally, we examine histone tail interactions with other internal chromatin components and PL2-6 at physiological (150 mM) (Fig. 6, *A–D*) and low (10 mM) (Fig. 6, *E–G*) monovalent salt concentrations for all PL2-6 chromatin systems. For free (*black*), monovalent PL2-6 (*magenta*), and bivalent PL2-6 (*purple*) chromatin systems, we show interactions of histone tails (H3, H4, $H2A_1$, H2B, and $H2A_2$) with parent cores (Fig. 6, *A* and *E*) and parent linkers (Fig. 6, *B* and *F*). For physiological salt only, we also show long-range interactions with nonparental cores (Fig. 6 *C*) and nonparental linkers (Fig. 6 *D*); such interactions are negligible for low salt (consistent with previous findings (24,38)). Finally, we show interactions of histone tails (H3, H4, $H2A_1$, H2B, and $H2A_2$) with PL2-6 at low salt (Fig. 6 *G*). At physiological salt, such interactions are transient and statistically unreliable.

Entropic interactions with histone tails is a key component in driving differential binding in open chromatin fibers

At low salt, open fibers have minimal long-range contacts (nonparental tail-core and tail-linker interactions, data not shown) but dominant short-range tail interactions with parental cores (Fig. 6 *E*). H4, H2B, and N-terminal $H2A_1$ tails in free chromatin have the largest interactions with their parental cores, similar to fibers at physiological salt but with slightly higher H3 intranucleosomal core interactions, as seen previously (24,38). Because of the proximity to entering/exiting DNA, the only significant interactions with parental linker DNA (Fig. 6 *F*) are in H3 and $H2A_2$ tails, which are reduced compared to physiological salt. This is largely consistent with previous studies at low salt (24,38).

Interactions of all tails with their parental cores are reduced in monovalent (*magenta*) PL2-6 complexes and even further in bivalent (*purple*) PL2-6 complexes. Similarly, although the tail-linker interactions are not significantly affected by the monovalent (*magenta*) PL2-6, they are disrupted by bivalent (*purple*) PL2-6 binding. These decreases in tail interactions with parental cores and parental linker DNA (Fig. 6, *E* and *F*) correspond directly in magnitude with increases in tail binding to PL2-6 for each specific tail (Fig. 6 *G*). The largest decreases in parental core interactions, from free to monovalent and from monovalent to bivalent (Fig. 6 *E*), occur for $H2A_1$ and H2B, which also show the largest increase in PL2-6 interactions from free to monovalent to bivalent (Fig. 6 *G*). Thus, differential binding of bivalent versus monovalent PL2-6 depends on this direct competition with internal fiber-tail contacts. We see similar patterns in the presence of LH (Fig. S9). However, linker DNA interactions with H3 tails are reduced through competition with LH for linker DNA contacts, freeing up H3 tails for greater interaction with parental cores in the absence of PL2-6.

The unfavorable repulsive electrostatics between positively charged tails and PL2-6, as well as the overall lack in tail specificity, suggests that the increased binding of bivalent PL2-6 is likely driven by greater entropic contributions to the free energy in bivalent over monovalent chromatin complexes. This results from the additional rotational degrees of freedom of the bivalent PL2-6 compared to the monovalent Fab. The effect is to increase the entropy for the histone tails when bound to the bivalent PL2-6 IgG compared to monovalent Fab tails.

Please cite this article in press as: Myers et al., Mesoscale Modeling of Nucleosome-Binding Antibody PL2-6: Mono- versus Bivalent Chromatin Complexes, Biophysical Journal (2020), https://doi.org/10.1016/j.bpj.2019.08.019

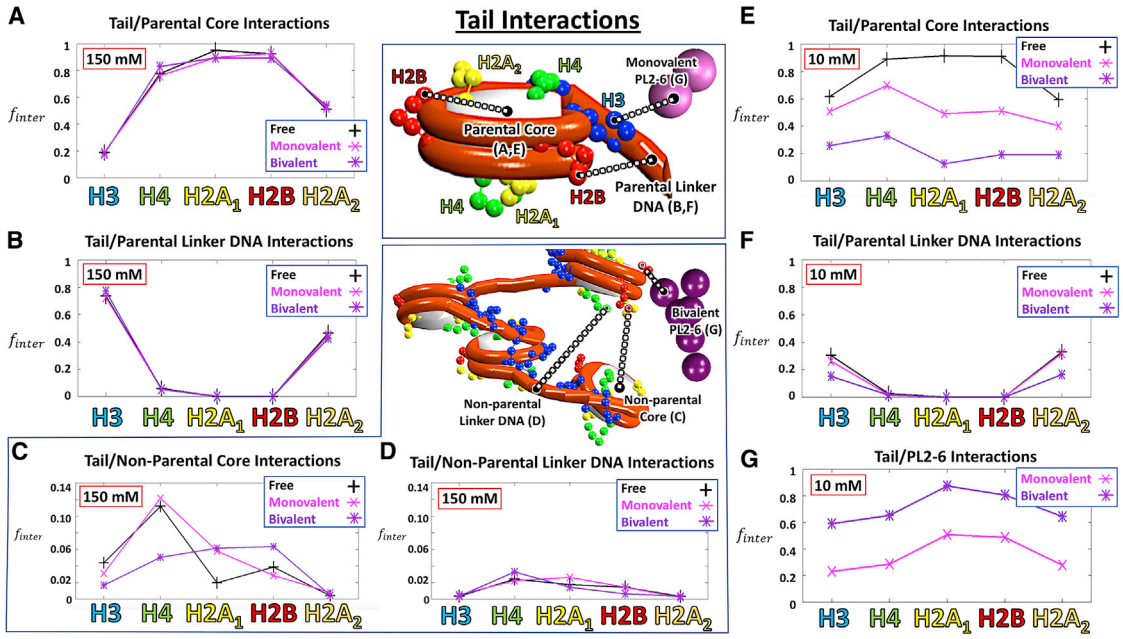

FIGURE 6 Tail interactions with chromatin and antibodies at physiological (*A–D*) and low salt (*E–G*). Interaction frequencies (f_{inter}) are evaluated by measuring the number of simulation frames for which pairwise distances between elements are ≤ 5 nm, sampled over the last 1 million frames of the simulation and normalized across all sampled frames. Tail interaction frequencies are averaged over both copies of each N-terminal tail for H3, H4, and H2B. $H2A_1$ and $H2A_2$ refer to N-terminal and C-terminal H2A tails, respectively. Distances are measured from the center of the end tail bead, from the geometric center of the entire nucleosome core, from the center of each linker bead, and from the center of the charged beads in both monovalent and bivalent systems. (*A*) Tail interactions with parental cores at physiological salt are shown. (*B*) Tail interactions with parental linker DNA at physiological salt are shown. (*C*) Tail interactions with nonparental cores at physiological salt are shown. (*D*) Tail interactions with nonparental linker DNA at physiological salt are shown. (*E*) Tail interactions with parental cores at low salt are shown. (*F*) Tail interactions with parental linker DNA at low salt are shown. (*G*) Tail interactions with antibodies at low salt are shown. Note that tail-nonparental core and nonparental linker DNA interactions are negligible at low salt. To see this figure in color, go online.

Tail interaction analyses (Fig. S10) comparing rigid to flexible bivalent PL2-6 complexes indicate similar results, with modest reductions in histone tail binding of flexible compared to rigid bivalent PL2-6 complexes, consistent with overall reduced chromatin interactions (Fig. S8). This suggests that differences in antibody type dominate over internal flexibility, lending our comparative study validity as a first approximation.

Transient PL2-6 interactions disrupt internal chromatin structure at physiological salt with LH-mediated differences

At physiological salt (Fig. 6 *A*), H4, H2A, and H2B tails show the greatest interactions with their parental cores. The H3 and C-terminal H2A ($H2A_2$) tails, on other hand, show the greatest contacts with parental linker DNA (Fig. 6 *B*) in free chromatin (*black*) because of their physical proximity to the entry/exit point on the nucleosome core. This is consistent with previous studies, except for a shift of $H2A_2$ toward greater parental linker interaction over parental cores (24,38). These predominant intranucleosomal interactions are minimally affected by introduction of monovalent and bivalent PL2-6 units, with changes for each tail (Fig. 6 *A*) correlating inversely to the changes in nonparental interactions (Fig. 6 *C*), as for free chromatin. Thus, although PL2-6 antibodies interact with chromatin only transiently at physiological salt, they induce conformational changes reflected by these shifts in internal chromatin interactions.

As in previous studies at 150 mM salt, modest but significant internucleosomal interactions are observed with nonparental cores and linker DNA (Fig. 6, *C* and *D*). Internal interactions in chromatin of monovalent and bivalent PL2-6 units affect these long-range tail interactions. Specifically, H3 and H4 interactions with nonparental cores, although not affected by monovalent PL2-6, are reduced in the presence of bivalent PL2-6 (Fig. 6 *C*). This is contrary to the effects of LHs, which have been shown to enhance internucleosomal contacts for H3 and H4 (24,38), consistent with the lower condensation observed for bivalent systems compared to free chromatin (Fig. 3 *B*). $H2A_1$ internucleosomal interactions are slightly elevated in both monovalent and bivalent systems relative to free chromatin, which is similar to previously observed effects of LH; however, H3 interactions with nonparental linker DNA are small (24,38).

With LH (Fig. S9, *part C*), bivalent PL2-6 enhances the effects of LH by increasing internucleosomal contacts of H3 and H4, whereas monovalent PL2-6 disrupts and opposes this LH-induced mechanism. Thus, internucleosomal contacts of H3 and H4 are repressed in the presence of monovalent PL2-6 but enhanced in the presence bivalent

Please cite this article in press as: Myers et al., Mesoscale Modeling of Nucleosome-Binding Antibody PL2-6: Mono- versus Bivalent Chromatin Complexes, Biophysical Journal (2020), https://doi.org/10.1016/j.bpj.2019.08.019

PL2-6 (Fig. S9). Through this cooperative mechanism, chromatin systems with both bivalent PL2-6 and LH are the most condensed (Fig. S4 *B*), indicating different conformational states for chromatin systems in the presence of bivalent versus monovalent PL2-6.

DISCUSSION

Our study has been motivated by the importance of complexes between antibodies and chromatin systems for various investigations, including therapeutic considerations. As a first step, we have combined mesoscale chromatin and coarse-grained protein models to simulate the binding of bivalent and monovalent forms of the anti-nucleosome IgG antibody (mAb PL2-6) to open flexible chromatin fibers in both low and physiological monovalent salt conditions, with and without LH.

We find that PL2-6 interactions help condense open chromatin fibers at low salt, with much greater binding observed for bivalent PL2-6 complexes compared to monovalent PL2-6 (Fig. 3). For such open fibers, we observe mechanisms similar to LH-induced condensation, reflecting similar changes in histone tail interactions. We observe similar interactions between the acidic patch and the antibodies for monovalent and bivalent complexes. However, conformational differences between monovalent and bivalent PL2-6 chromatin complexes lead to an overall decreased acidic-patch affinity in bivalent compared to monovalent systems due to decreased nucleosome core interactions with bivalent PL2-6. For these open chromatin fibers, competition for internal chromatin interactions accounts for differential antibody binding between bivalent and monovalent PL2-6 complexes. Under these conditions, differences in Fab binding to histone tails play the largest role in driving differential binding. Such energetically unfavorable tail-antibody interactions, with relatively low specificity across all histone tails, suggest that entropy differences between histone tail binding of monovalent and bivalent PL2-6 drive the observed difference in binding within open fibers. Entropy differences due to changes in histone tail contacts (39) and H1 LH conformations (40) have been recently implicated in altering nucleosomal structure and binding. A growing number of studies based on liquid-liquid phase separation also demonstrate that entropic forces can drive observed differences in genomic organization (41–43).

For condensed fibers at physiological salt, slight changes in chromatin fiber condensation are mediated through mechanisms resembling LH-chromatin interactions. These involve changes in internucleosomal histone tail interactions and charge screening induced by both monovalent and bivalent PL2-6. Whereas LH tends to decrease H3 and H4 interactions with parental cores, bivalent PL2-6 increases such internucleosomal contacts.

For most systems, adding LH results in less-dramatic differences between monovalent and bivalent complexes. However, at physiological salt, monovalent PL2-6 works in opposition to LH to change in internucleosomal interactions, whereas bivalent PL2-6 works in concert with LH to further condense chromatin fibers.

After completion of our study, a cryo-electron microscopy structure was reported for a mononucleosome bound to PL2-6-derived single-chain antibody fragment (scFv). The antibody unit was intended to stabilize the nucleosome particle and increase its resolution. The complex shows specific binding of scFv to the acidic-patch residues of H2A/H2B and suggests few overall changes to nucleosomal structure (44). These findings are consistent with previous evidence supporting PL2-6 binding at the acidic patch, facilitated by chemically specific and electrostatic interactions with arginines found in the PL2-6 CDR binding loops. As is well-known for LH binding (45), however, the behavior of mononucleosomes is very different from that of nucleosome arrays, as modeled here, and thus our models are not directly comparable. Moreover, cryo-electron microscopy reconstructions, as with crystallographic structures, represent averages of static structures (~500,000 particle projections here). Capturing the transient states of highly dynamic complexes for elucidating related molecular mechanisms may require computational modeling (46). The models developed here can thus remedy such issues to provide additional structural insights into fiber-scFv complexes.

Mesoscale modeling, as described here and extended to genes (47,48), could eventually help explain how differences in internal chromatin structure might drive experimentally observed differential binding of bivalent versus monovalent PL2-6 to address the epichromatin hypothesis. For now, our results likely inform conformational changes that may precede final chromatin binding captured in current staining experiments. Because immunostaining is conducted on formaldehyde-fixed and detergent permeabilized cells, molecular motion of the chromatin is somewhat suppressed, and space for antibody diffusion may be reduced with the antibody incubations performed in physiological PBS buffer (2,11,12). It would also be interesting to test the predictions here within isolated and unfixed cell nuclei incubated with mono- and bivalent PL2-6. The aggregate knowledge about the mAb PL2-6 antibody system suggests that "molecular rulers" could eventually be synthesized by employing bivalent Fab fragments connected by rigid bridges as probes for different chromatin conformations, both in vitro and in vivo. Ongoing modeling and experiments could help further bridge these intriguing phenomena to investigate these important problems.

SUPPORTING MATERIAL

Supporting Material can be found online at https://doi.org/10.1016/j.bpj.2019.08.019.

Please cite this article in press as: Myers et al., Mesoscale Modeling of Nucleosome-Binding Antibody PL2-6: Mono- versus Bivalent Chromatin Complexes, Biophysical Journal (2020), https://doi.org/10.1016/j.bpj.2019.08.019

AUTHOR CONTRIBUTIONS

C.G.M. and T.S. designed the research. C.G.M. performed the simulations and analyzed the data. C.G.M., T.S., D.E.O., and A.L.O. wrote the manuscript.

ACKNOWLEDGMENTS

We thank Robyn Stanfield for providing the PL2-6 Fab homology model used for electrostatic calculations. D.E.O. and A.L.O. gratefully acknowledge the University of New England, College of Pharmacy for supporting our research and Bates College and Travis Gould (Department of Physics and Astronomy) for supporting our joint research.

This work was supported by the National Institutes of Health, National Institute of General Medical Sciences awards R01-GM055264 and R35-GM122562 and Phillip-Morris USA and Phillip-Morris International to T.S. Simulations were performed on the New York University high-performance computing cluster Prince and the Schlick group's Schulten cluster.

REFERENCES

1. Seredkina, N., J. Van Der Vlag, …, O. P. Rekvig. 2013. Lupus nephritis: enigmas, conflicting models and an emerging concept. *Mol. Med.* 19:161–169.
2. Olins, A. L., M. Langhans, …, D. E. Olins. 2011. An epichromatin epitope: persistence in the cell cycle and conservation in evolution. *Nucleus.* 2:47–60.
3. Fyodorov, D. V., B. R. Zhou, …, Y. Bai. 2018. Emerging roles of linker histones in regulating chromatin structure and function. *Nat. Rev. Mol. Cell Biol.* 19:192–206.
4. Chen, T., and S. Y. Dent. 2014. Chromatin modifiers and remodellers: regulators of cellular differentiation. *Nat. Rev. Genet.* 15:93–106.
5. Klemm, S. L., Z. Shipony, and W. J. Greenleaf. 2019. Chromatin accessibility and the regulatory epigenome. *Nat. Rev. Genet.* 20:207–220.
6. Lai, W. K. M., and B. F. Pugh. 2017. Understanding nucleosome dynamics and their links to gene expression and DNA replication. *Nat. Rev. Mol. Cell Biol.* 18:548–562.
7. Portillo-Ledesma, S., and T. Schlick. 2019. Bridging chromatin structure and function over a range of experimental spatial and temporal scales by molecular modeling. *Wiley Interdiscip. Rev. Comput. Mol. Sci* Published online August 6, 2019. https://doi.org/10.1002/wcms.1434.
8. Hedberg, A., E. S. Mortensen, and O. P. Rekvig. 2011. Chromatin as a target antigen in human and murine lupus nephritis. *Arthritis Res. Ther.* 13:214.
9. Hedrich, C. M. 2019. Pharmacoepigenetics of systemic lupus erythematosus. *In* Pharmacoepigenetics. R. Cacabelos, ed. Academic Press, pp. 597–608.
10. Olins, D. E., and A. L. Olins. 2018. Epichromatin and chromomeres: a 'fuzzy' perspective. *Open Biol.* 8:180058.
11. Olins, A. L., N. Ishaque, …, D. E. Olins. 2014. Retrotransposon Alu is enriched in the epichromatin of HL-60 cells. *Nucleus.* 5:237–246.
12. Gould, T. J., K. Tóth, …, D. E. Olins. 2017. Defining the epichromatin epitope. *Nucleus.* 8:625–640.
13. Luque, A., R. Collepardo-Guevara, …, T. Schlick. 2014. Dynamic condensation of linker histone C-terminal domain regulates chromatin structure. *Nucleic Acids Res.* 42:7553–7560.
14. Perišić, O., S. Portillo-Ledesma, and T. Schlick. 2019. Sensitive effect of linker histone binding mode and subtype on chromatin condensation. *Nucleic Acids Res.* 47:4948–4957.
15. Losman, M. J., T. M. Fasy, …, M. Monestier. 1992. Monoclonal autoantibodies to subnucleosomes from a MRL/Mp(-)+/+ mouse. Oligoclonality of the antibody response and recognition of a determinant composed of histones H2A, H2B, and DNA. *J. Immunol.* 148:1561–1569.
16. Stanfield, R. L., and I. A. Wilson. 2009. Antibody molecular structure. *In* Therapeutic Monoclonal Antibodies: From Bench to Clinic. Z. An, ed. John Wiley & Sons, Ltd, pp. 51–66.
17. Falk, S. J., L. Y. Guo, …, B. E. Black. 2015. Chromosomes. CENP-C reshapes and stabilizes CENP-A nucleosomes at the centromere. *Science.* 348:699–703.
18. Barbera, A. J., J. V. Chodaparambil, …, K. M. Kaye. 2006. Kaposi's sarcoma-associated herpesvirus LANA hitches a ride on the chromosome. *Cell Cycle.* 5:1048–1052.
19. Roussel, L., M. Erard, …, J. P. Girard. 2008. Molecular mimicry between IL-33 and KSHV for attachment to chromatin through the H2A-H2B acidic pocket. *EMBO Rep.* 9:1006–1012.
20. Barbera, A. J., J. V. Chodaparambil, …, K. M. Kaye. 2006. The nucleosomal surface as a docking station for Kaposi's sarcoma herpesvirus LANA. *Science.* 311:856–861.
21. Dann, G. P., G. P. Liszczak, …, T. W. Muir. 2017. ISWI chromatin remodellers sense nucleosome modifications to determine substrate preference. *Nature.* 548:607–611.
22. Baker, N. A., D. Sept, …, J. A. McCammon. 2001. Electrostatics of nanosystems: application to microtubules and the ribosome. *Proc. Natl. Acad. Sci. USA.* 98:10037–10041.
23. Jurrus, E., D. Engel, …, N. A. Baker. 2018. Improvements to the APBS biomolecular solvation software suite. *Protein Sci.* 27:112–128.
24. Arya, G., and T. Schlick. 2006. Role of histone tails in chromatin folding revealed by a mesoscopic oligonucleosome model. *Proc. Natl. Acad. Sci. USA.* 103:16236–16241.
25. Collepardo-Guevara, R., and T. Schlick. 2014. Chromatin fiber polymorphism triggered by variations of DNA linker lengths. *Proc. Natl. Acad. Sci. USA.* 111:8061–8066.
26. Perišić, O., R. Collepardo-Guevara, and T. Schlick. 2010. Modeling studies of chromatin fiber structure as a function of DNA linker length. *J. Mol. Biol.* 403:777–802.
27. Beard, D. A., and T. Schlick. 2001. Modeling salt-mediated electrostatics of macromolecules: the discrete surface charge optimization algorithm and its application to the nucleosome. *Biopolymers.* 58:106–115.
28. Zhang, Q., D. A. Beard, and T. Schlick. 2003. Constructing irregular surfaces to enclose macromolecular complexes for mesoscale modeling using the discrete surface charge optimization (DISCO) algorithm. *J. Comput. Chem.* 24:2063–2074.
29. Davey, C. A., D. F. Sargent, …, T. J. Richmond. 2002. Solvent mediated interactions in the structure of the nucleosome core particle at 1.9 a resolution. *J. Mol. Biol.* 319:1097–1113.
30. Bharath, M. M., N. R. Chandra, and M. R. Rao. 2002. Prediction of an HMG-box fold in the C-terminal domain of histone H1: insights into its role in DNA condensation. *Proteins.* 49:71–81.
31. Bharath, M. M., N. R. Chandra, and M. R. Rao. 2003. Molecular modeling of the chromatosome particle. *Nucleic Acids Res.* 31:4264–4274.
32. Bascom, G. D., K. Y. Sanbonmatsu, and T. Schlick. 2016. Mesoscale modeling reveals hierarchical looping of chromatin fibers near gene regulatory elements. *J. Phys. Chem. B.* 120:8642–8653.
33. Calero-Rubio, C., R. Ghosh, …, C. J. Roberts. 2018. Predicting protein-protein interactions of concentrated antibody solutions using dilute solution data and coarse-grained molecular models. *J. Pharm. Sci.* 107:1269–1281.
34. Calero-Rubio, C., A. Saluja, and C. J. Roberts. 2016. Coarse-grained antibody models for "weak" protein-protein interactions from low to high concentrations. *J. Phys. Chem. B.* 120:6592–6605.
35. Woldeyes, M. A., C. Calero-Rubio, …, C. J. Roberts. 2017. Predicting protein interactions of concentrated globular protein solutions using colloidal models. *J. Phys. Chem. B.* 121:4756–4767.
36. De Michele, C., P. De Los Rios, …, F. Piazza. 2016. Simulation and theory of antibody binding to crowded antigen-covered surfaces. *PLOS Comput. Biol.* 12:e1004752.

37. Vidarsson, G., G. Dekkers, and T. Rispens. 2014. IgG subclasses and allotypes: from structure to effector functions. *Front. Immunol.* 5:520.

38. Arya, G., and T. Schlick. 2009. A tale of tails: how histone tails mediate chromatin compaction in different salt and linker histone environments. *J. Phys. Chem. A.* 113:4045–4059.

39. Parsons, T., and B. Zhang. 2019. Critical role of histone tail entropy in nucleosome unwinding. *J. Chem. Phys.* 150:185103.

40. Turner, A. L., M. Watson, …, K. Stott. 2018. Highly disordered histone H1-DNA model complexes and their condensates. *Proc. Natl. Acad. Sci. USA.* 115:11964–11969.

41. Lee, S. S., S. Tashiro, …, R. Kobayashi. 2017. A new application of the phase-field method for understanding the mechanisms of nuclear architecture reorganization. *J. Math. Biol.* 74:333–354.

42. Wang, N., and C. Liu. 2019. Implications of liquid-liquid phase separation in plant chromatin organization and transcriptional control. *Curr. Opin. Genet. Dev.* 55:59–65.

43. Finan, K., P. R. Cook, and D. Marenduzzo. 2011. Non-specific (entropic) forces as major determinants of the structure of mammalian chromosomes. *Chromosome Res.* 19:53–61.

44. Zhou, B. R., K. N. S. Yadav, …, P. Zhang. 2019. Atomic resolution cryo-EM structure of a native-like CENP-A nucleosome aided by an antibody fragment. *Nat. Commun.* 10:2301.

45. Fang, H., S. Wei, …, J. J. Hayes. 2016. Chromatin structure-dependent conformations of the H1 CTD. *Nucleic Acids Res.* 44:9131–9141.

46. Srivastava, A., T. Nagai, …, F. Tama. 2018. Role of computational methods in going beyond X-ray crystallography to explore protein structure and dynamics. *Int. J. Mol. Sci.* 19:3401.

47. Bascom, G. D., C. Myers, and T. Schlick. 2019. Mesoscale modeling reveals formation of an epigenetically driven HOXC gene hub. *Proc. Natl. Acad. Sci. USA.* 116:4955–4962.

48. de Pierro, M. D. 2019. Inner workings of gene folding. *Proc. Natl. Acad. Sci. USA.* 116:4774–4775.

Biophysical Journal, Volume *118*

Supplemental Information

Mesoscale Modeling of Nucleosome-Binding Antibody PL2-6: Mono- versus Bivalent Chromatin Complexes

Christopher G. Myers, Donald E. Olins, Ada L. Olins, and Tamar Schlick

Additional Methods

Model Constituents

Histone tails are modeled at a resolution of 5 amino acids per bead. Similarly, LHs are represented as 6 beads for the globular head (GH) and 22 beads for the flexible C-terminal Domain (CTD) as described in Ref. (1). See Ref. (2) for further model details and validation of equilibrium and dynamic properties.

Initial Starting Configurations

The initial 3D structure for all chromatin fibers are generated as ideal zigzag conformations with the long fiber axis oriented parallel to the z-axis. The z-rise per nucleosome (distance between successive nucleosomes along the long fiber axis) and fiber width (distance between successive nucleosomes when viewed in the plane perpendicular to the fiber axis) are assigned values proportional to the DNA linker length between nucleosomes such that DNA/DNA linker bead distances are less than the DNA bead radius (3 nm). Any overlaps between cores or linker DNA beads are removed. Nucleosomes are initially oriented perpendicular to the central axis, according to the zigzag structure found to be optimal in Ref. (3) (Fig. S1) due to stabilization by the H3 tail interactions with linker DNA.

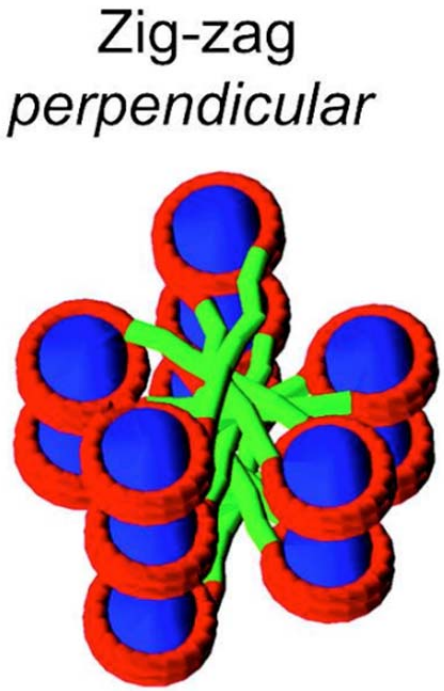

Figure S1. Initial perpendicular zigzag chromatin fiber structure (Ref. 3).

Initial coordinates for all monovalent and bivalent antibodies are placed along an approximate cylinder of 100 nm from each nucleosome, with 3 antibodies (each spaced at an additional 20 nm for the second and third antibodies per nucleosome). The first of each antibody triplet per nucleosome is translated 100 nm from the nucleosome center to the antibody center, along the *line of nodes*—defined as the x'-axis in the rotated reference frame determined by each nucleosome's initial Euler angle coordinate frame. Each monovalent antibody's long 'Fab' axis is oriented *parallel* with the nucleosome's *line of nodes* (Fig. S2) while each bivalent antibody's long 'Fc' axis is oriented *perpendicular* to the nucleosome's *line of nodes* (Fig. S3).

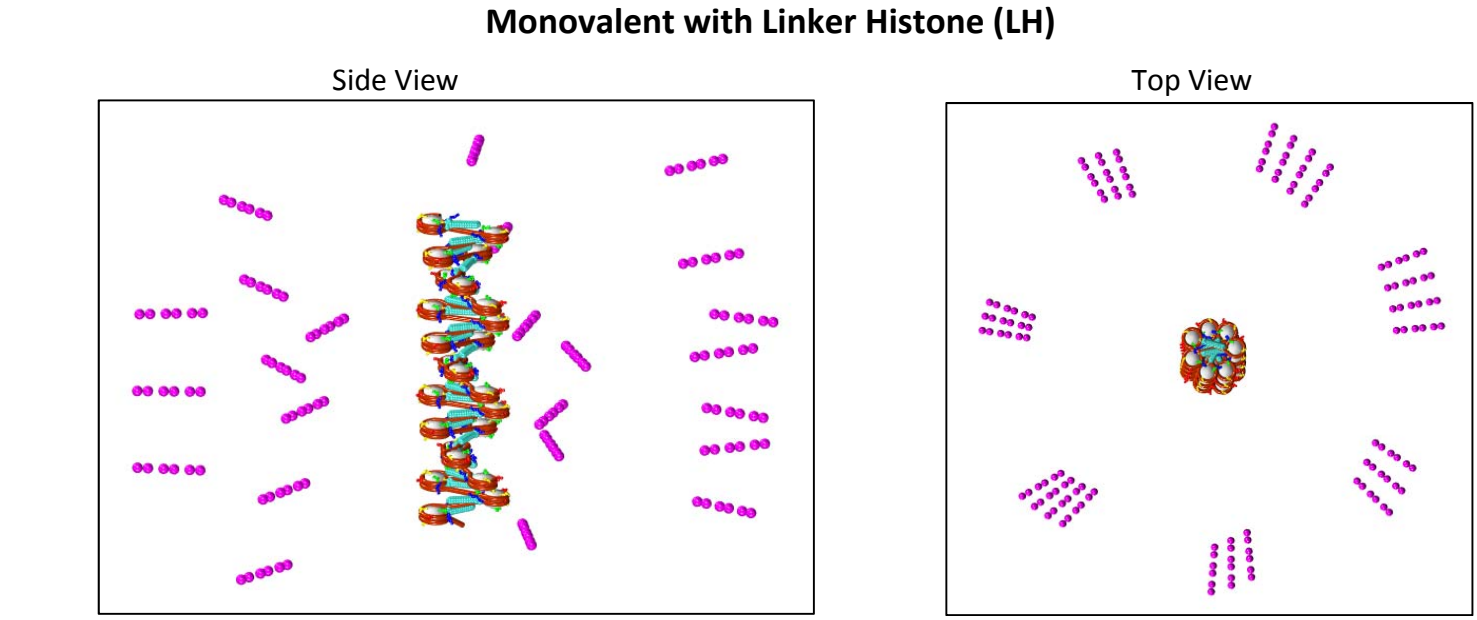

Figure S2. Initial positions for zigzag chromatin fibers with monovalent antibodies used in our MC simulations. Representative example with linker histone.

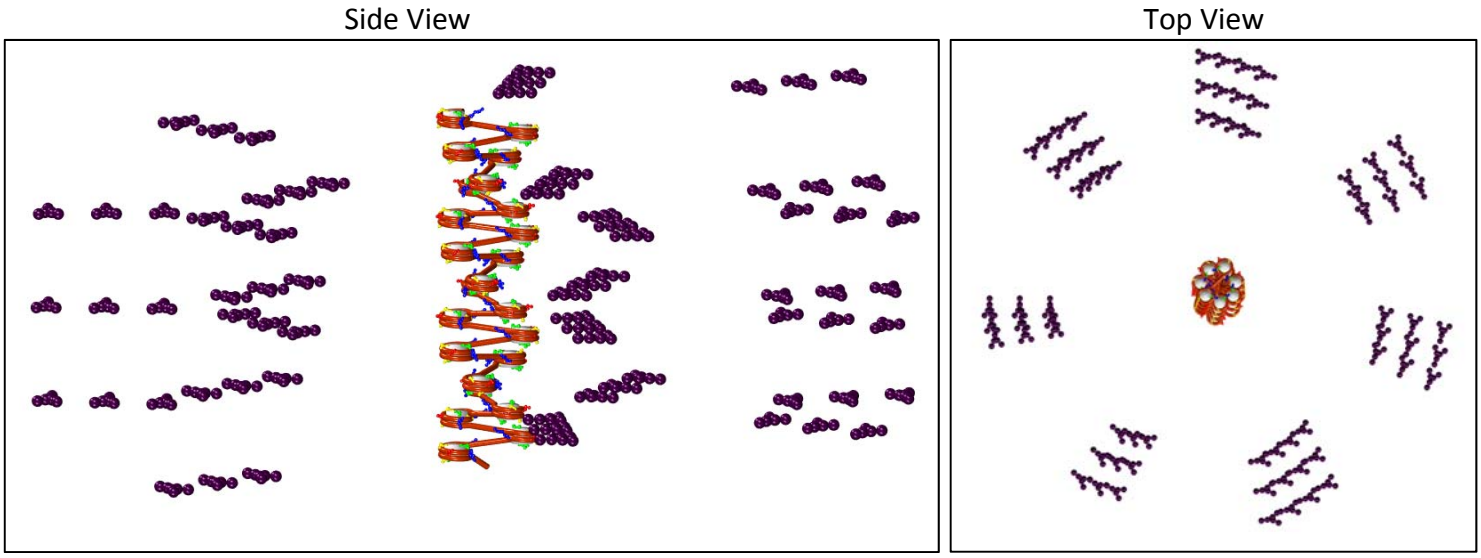

Figure S3. Initial positions for zigzag chromatin fibers with bivalent antibodies used in our MC simulations. Representative example without linker histone.

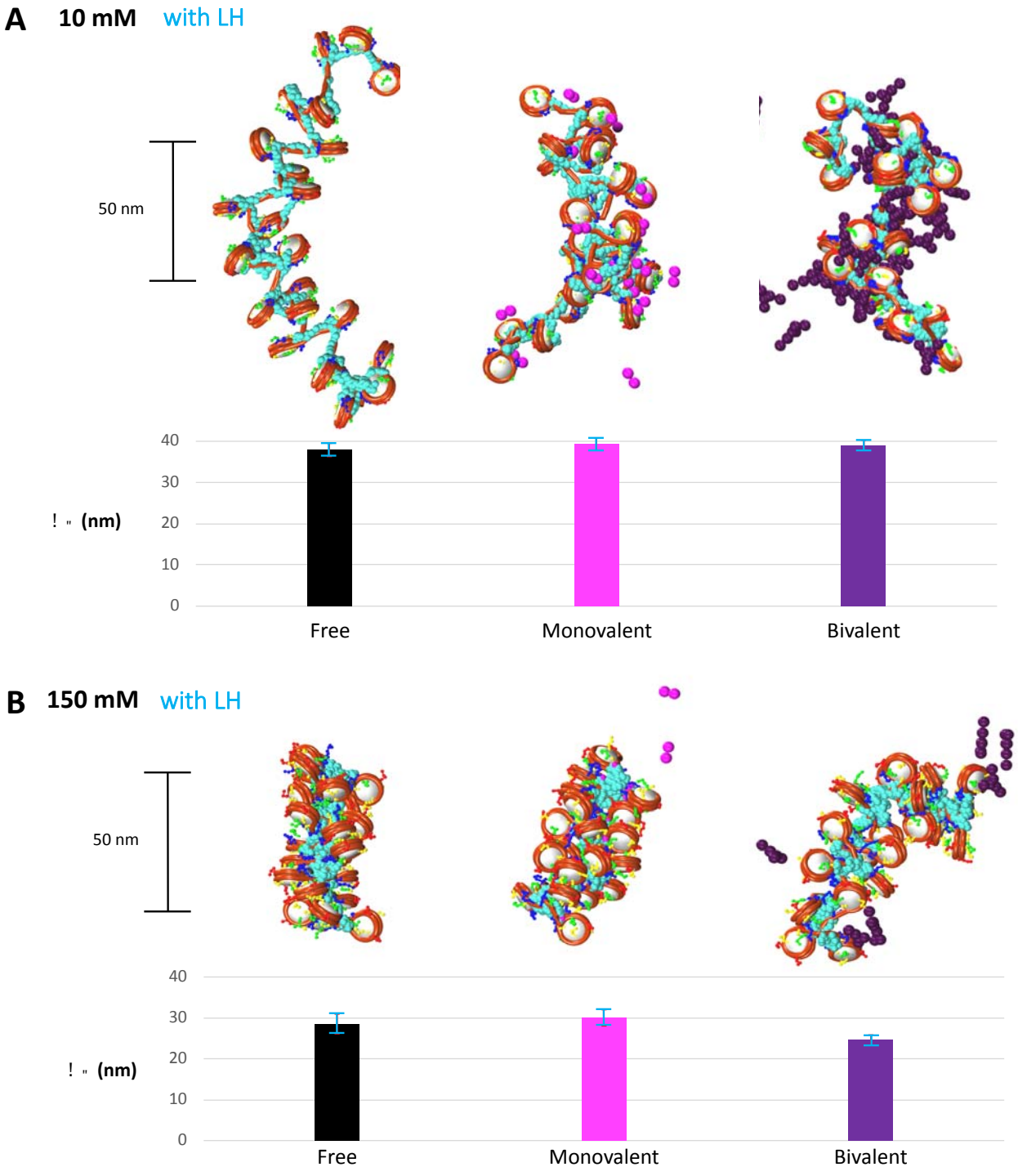

Figure S4. Snapshots of representative fibers from antibody/chromatin systems with linker histone (LH). All fibers consist of 24 nucleosomes and start from idealized zigzag configurations (Figs. S1-S2). For each condition (low salt / physiological salt) we show results for free fiber, monovalent PL2-6 Fab complex, and bivalent PL2-6 complex. Radii of gyration (R_G) of chromatin fibers are shown in nanometers (nm) for free (black), monovalent (magenta), and bivalent (purple) systems, with standard deviations shown as blue error bars. (A) Low salt. (B) Physiological salt. Both with LH.

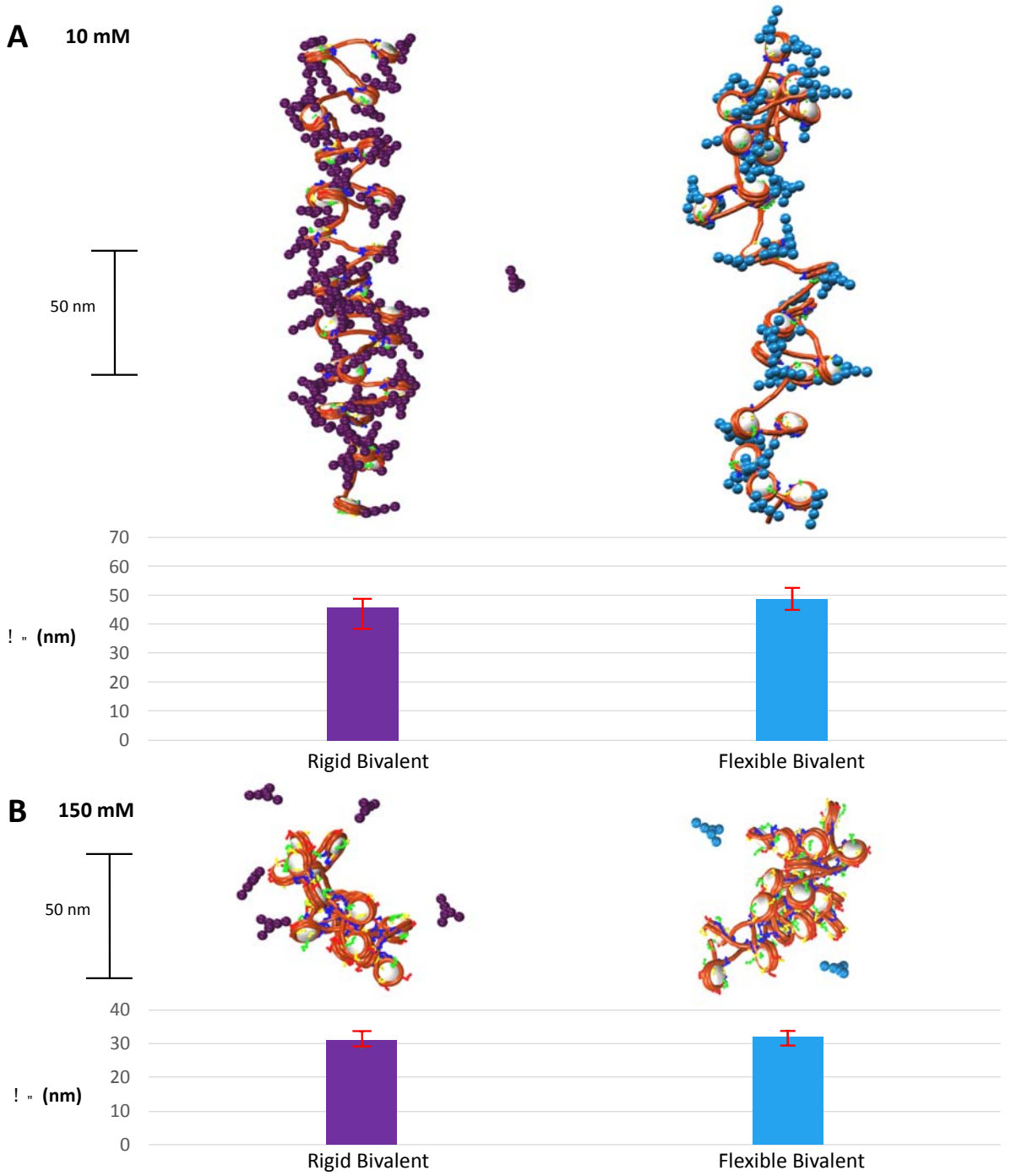

Figure S5. Snapshots of representative fibers of rigid vs flexible bivalent PL2-6/chromatin systems without LH. All fibers consist of 24 nucleosomes and start from idealized zigzag configurations (Figs. S1-S2). For each condition (low salt / physiological salt) we show results for rigid versus bivalent PL2-6 complexes. Radii of gyration (R_G) of chromatin fibers are shown in nanometers (nm) for rigid (purple) bivalent PL2-6 and flexible (blue) bivalent PL2-6 systems, with standard deviations shown as red error bars. (A) Low salt. (B) Physiological salt. Both without LH.

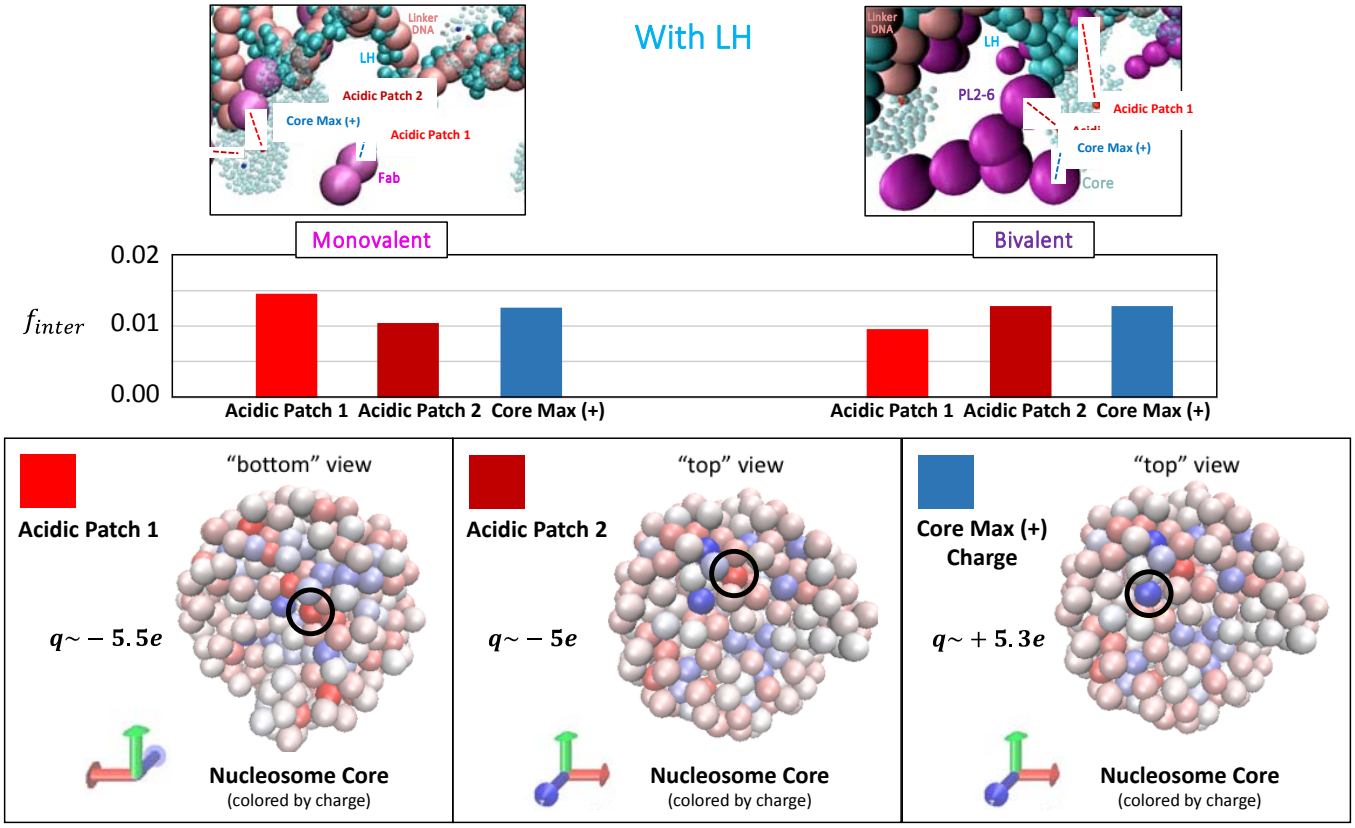

Figure S6. PL2-6 interactions with specific regions of the nucleosome core with LH. The three regions are the two sides of the negatively-charged acidic patch (arbitrarily labeled as Acidic Patch 1 and 2), and the largest positive charge on the nucleosome surface (Core Max (+)). Interaction frequencies (f_{inter}) are evaluated by measuring the number of simulation frames for which pairwise distances between elements are ≤5 nm, sampled over the last 1 million frames of the simulation and normalized across all sampled frames. Pairwise distances are measured from the center of the specified charged bead on the nucleosome core and from the center of the charged beads in both monovalent and bivalent systems. Acidic Patch 1 (red), Acidic Patch 2 (dark red), Core Max (+) Charge (blue).

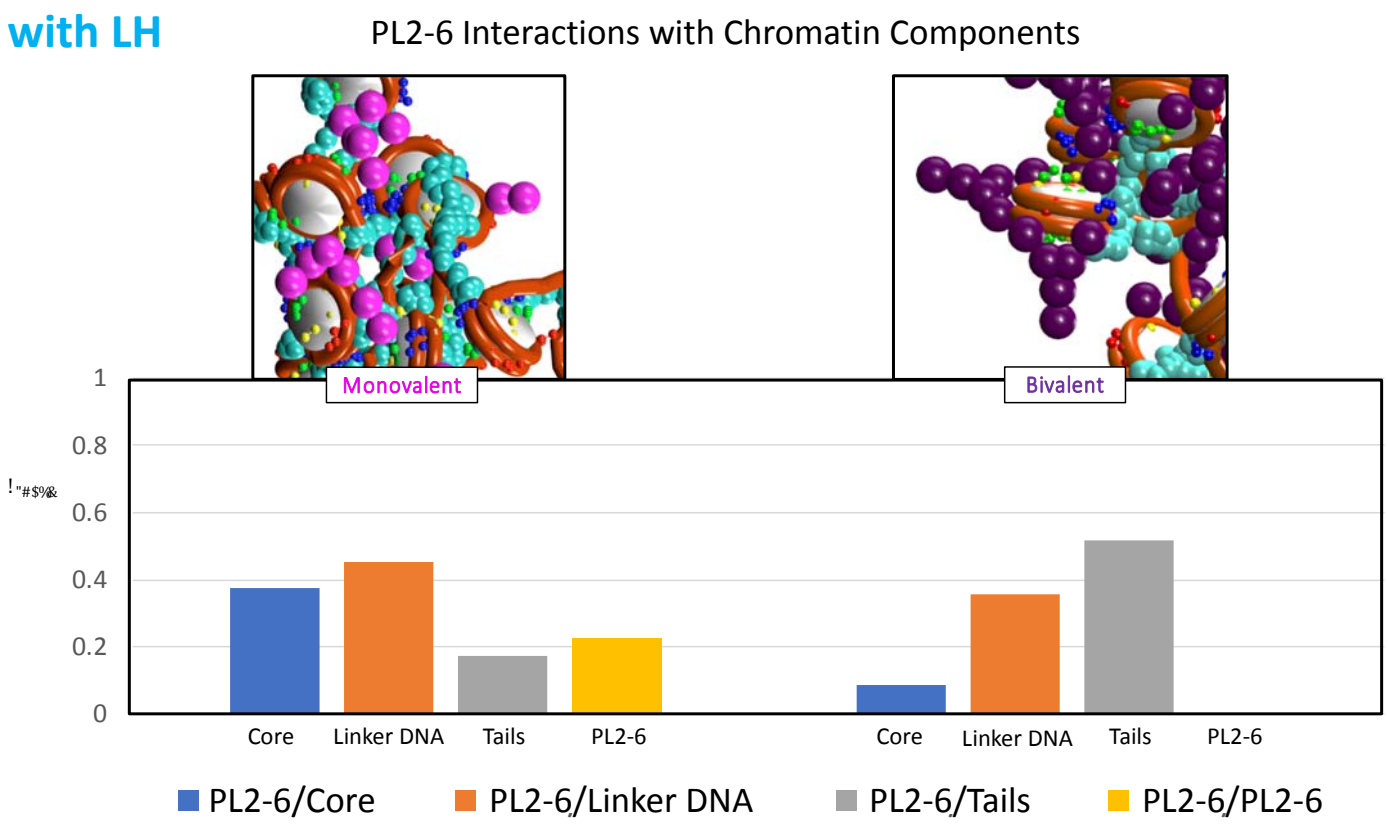

Figure S7. Overall antibody interactions with elements of open chromatin fiber (cores, DNA linkers, tails, and other PL2-6 antibodies) at low salt with LH. Interaction frequencies (f_{inter}) are evaluated by measuring the number of simulation frames for which pairwise distances between elements are ≤5 nm, sampled over the last 1 million frames of the simulation and normalized across all sampled frames. Interactions are averaged over all elements in the fiber for each category (core, linkers, tails, Fabs). Pairwise distances are measured from the center of the end tail bead, from the geometric center of the entire nucleosome core, from the center of each linker bead, and from the center of the charged beads in both monovalent and bivalent systems.

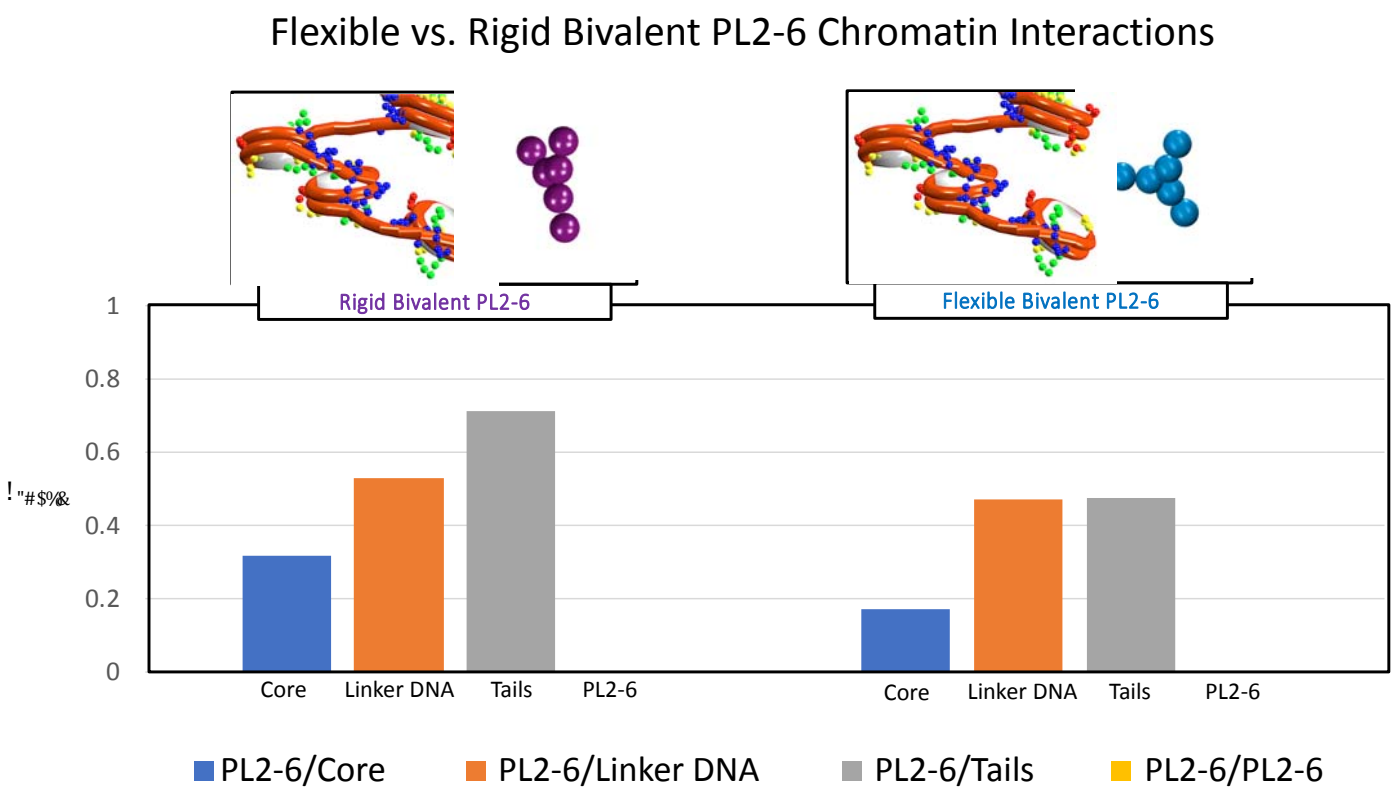

Figure S8. Rigid versus Bivalent PL2-6 Overall Chromatin Interactions. Comparing overall chromatin/antibody interactions between rigid versus flexible bivalent PL2-6 with elements of open chromatin fiber (cores, DNA linkers, tails, and other PL2-6 antibodies) at low salt. Interaction frequencies (f_{inter}) are evaluated by measuring the number of simulation frames for which pairwise distances between elements are ≤5 nm, sampled over the last 1 million frames of the simulation and normalized across all sampled frames. Interactions are averaged over all elements in the fiber for each category (cores, linker DNA, tails, Fabs). Pairwise distances are measured from the center of the end tail bead, from the geometric center of the entire nucleosome core, from the center of each linker bead, and from the center of the charged beads in both monovalent and bivalent systems.

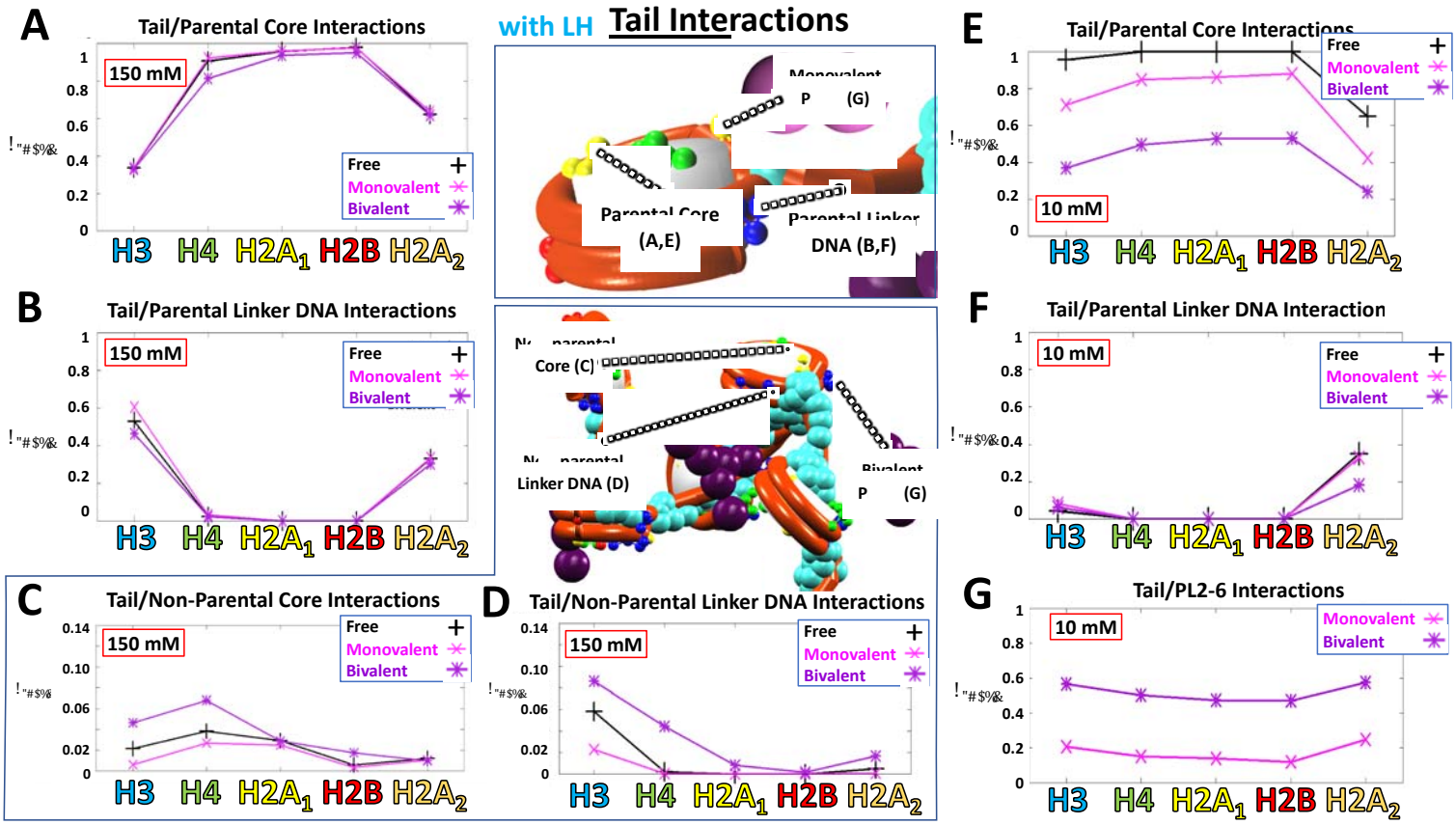

Figure S9. Tail interactions with chromatin and antibodies at physiological and low salt. Interaction frequencies (f_{inter}) are evaluated by measuring the number of simulation frames for which pairwise distances between elements are ≤5 nm, sampled over the last 1 million frames of the simulation and normalized across all sampled frames. Tail interaction frequencies are averaged over both copies of each C-terminal tail for H3, H4, and H2B. H2A1 and H2A2 refer to C-terminal and N-terminal H2A tails, respectively. Distances are measured from the center of the end tail bead, from the geometric center of the entire nucleosome core, from the center of each linker bead, and from the center of the charged beads in both monovalent and bivalent systems. (A) Tail interactions with parental cores at low salt. (B) Tail interactions with parental cores at low salt. (C) Tail interactions with parental linker DNA at physiological salt. (D) Tail interactions with parental linker DNA at low salt. (E) Tail interactions with nonparental cores at physiological salt. (F) Tail interactions with nonparental linker DNA at physiological salt. (G) Tail interactions with antibodies at low salt.

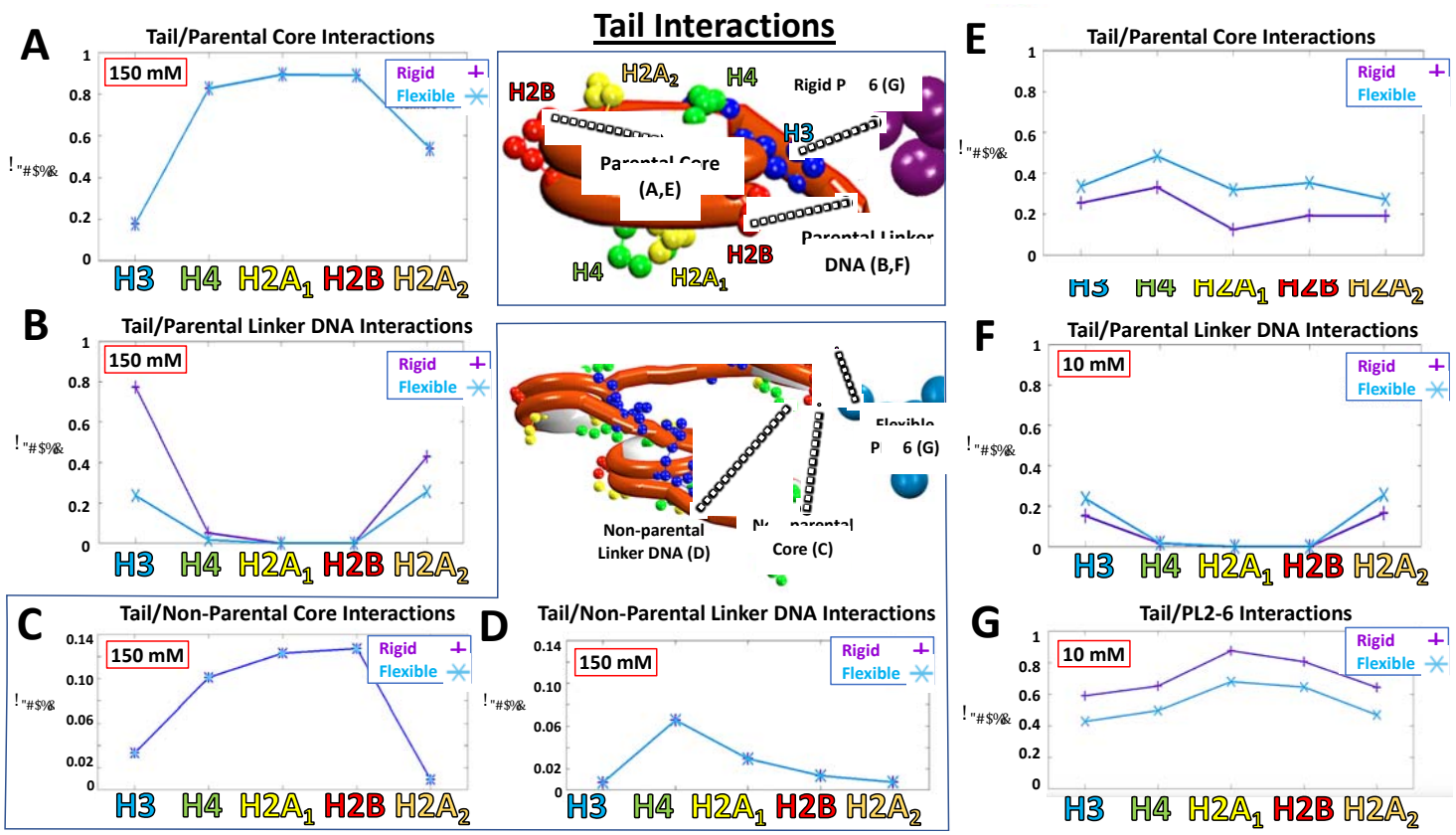

Figure S10. Flexible versus Rigid Bivalent PL2-6 IgG. Interaction frequencies (f_{inter}) are evaluated by measuring the number of simulation frames for which pairwise distances between elements are ≤5 nm, sampled over the last 1 million frames of the simulation and normalized across all sampled frames. Tail interaction frequencies are averaged over both copies of each C-terminal tail for H3, H4, and H2B. H2A1 and H2A2 refer to C-terminal and N-terminal H2A tails, respectively. Distances are measured from the center of the end tail bead, from the geometric center of the entire nucleosome core, from the center of each linker bead, and from the center of the charged beads in both monovalent and bivalent systems. (A) Tail interactions with parental cores at low salt. (B) Tail interactions with parental linker DNA at physiological salt. (C) Tail interactions with nonparental cores at physiological salt. (D) Tail interactions with nonparental linker DNA at physiological salt. (E) Tail interactions with parental cores at low salt. (F) Tail interactions with parental linker DNA at low salt. (G) Tail interactions with antibodies at low salt.

References:

1. Luque A, Collepardo-Guevara R, Grigoryev S, Schlick T (2014) Dynamic condensation of linker histone C-terminal domain regulates chromatin structure. Nucl. Acids Res. 42:7553–7560.
2. Bascom G, Schlick T (2018) Chromatin fiber folding directed by cooperative histone tail acetylation and linker histone binding. Biophys. J. 114(10):2376–2385.
3. Sun J, Zhang Q, Schlick T (2005) Electrostatic mechanism of nucleosomal array folding revealed by computer simulation. Proc. Natl. Acad. Sci. USA 102:8180—8185.